Channel Coupling Dynamics of Deep-Lying Orbitals in Molecular High-Harmonic Generation

Zheng Shu,[1,*] Hongjing Liang,[2,*] Yichen Wang,[2] Shilin Hu,[3,†] Shi Chen,[4] Haifeng Xu,[2] Ri Ma,[2,‡] Dajun Ding,[2] and Jing Chen[1,5,§]

[1]*Institute of Applied Physics and Computational Mathematics, P.O. Box 8009, Beijing 100088, China*
[2]*Institute of Atomic and Molecular Physics, Jilin University, Changchun 130012, China*
[3]*Guangdong Provincial Key Laboratory of Quantum Metrology and Sensing School of Physics and Astronomy, Sun Yat-Sen University (Zhuhai Campus), Zhuhai 519082, China*
[4]*Center for Applied Physics and Technology, HEDPS, and School of Physics, Peking University, Beijing 100871, China*
[5]*Shenzhen Key Laboratory of Ultraintense Laser and Advanced Material Technology, Center for Advanced Material Diagnostic Technology, and College of Engineering Physics, Shenzhen Technology University, Shenzhen 518118, China*

(Received 18 September 2021; revised 15 February 2022; accepted 15 April 2022; published 6 May 2022)

Investigation on structures in the high-harmonic spectrum has provided profuse information of molecular structure and dynamics in intense laser fields, based on which techniques of molecular ultrafast dynamics imaging have been developed. Combining *ab initio* calculations and experimental measurements on the high-harmonic spectrum of the CO_2 molecule, we find a novel dip structure in the low-energy region of the harmonic spectrum which is identified as fingerprints of participation of deeper-lying molecular orbitals in the process and decodes the underlying attosecond multichannel coupling dynamics. Our work sheds new light on the ultrafast dynamics of molecules in intense laser fields.

DOI: 10.1103/PhysRevLett.128.183202

The overall high-harmonic (HH) spectrum emitted from atomic or molecular gases exposed to intense femtosecond laser pulses can be understood by the semiclasscial three-step picture: ionization, propagation, and photorecombination [1,2]. Nevertheless, various fine structures (dips and humps) in the HH spectrum have been intensively investigated, which greatly advanced our understanding of the structure and dynamics of its generating medium [3–6]. The progress triggers development of imaging methods to explore ultrafast dynamics of atoms, molecules, and materials on an attosecond timescale [7–11].

In atomic high-harmonic generation (HHG), the Cooper minimum as a result of interference between partial *s* and *d* waves of the continuum states is found to be responsible for the dip at about 55 eV observed in the HH spectrum of Ar [12], and a broad hump in the HH spectrum of the Xe atom is attributed to giant resonance [13]. In molecular HHG, two-center interference is used to explain the intensity-independent minimum appearing in the HH spectrum of H_2 [14,15]; however, the underlying mechanism of minimum observed in the HH spectrum of CO_2, which is intensity dependent, causes strong debate [16–19]. Later, Smirnova *et al.* provided compelling evidence that the interference minima in the harmonic spectra of CO_2 have primarily a dynamical rather than a geometrical origin, where the spectral minimum comes from interference between two cationic states $\tilde{X}$ and $\tilde{B}$ where an electron is ionized from the highest-occupied molecular orbital (HOMO) and HOMO-2, respectively [20]. However, the contributions from the deeper molecular orbitals are ignored. In the investigations of hydrogen molecular ion H_2^+ at extended internuclear distances, the nonadiabatic electron response to intense laser fields caused by the coupling between the ground and first excited states leaves the fingerprint of transiently suppressed ionization in the HHG spectra [21,22], which reveals the nonadiabatic electron dynamics on an attosecond timescale.

Now it is well accepted that molecular HHG inevitably involves multielectron effects including multichannel [20,23–26], correlation [27–29], multichannel resonance [30], and cross-channel and channel coupling [31,32]. Needless to say, understanding of these complex dynamics is indispensable for techniques to image molecular orbitals, especially for deep-lying orbitals [33]. For the CO_2 molecule, though having been intensively studied, its complicated dynamics in an intense laser field remains not fully understood. Angle-resolved ionization yields of CO_2 in an intense laser field causes long-term debate [34–37]. In the HHG of CO_2, the structure interference in photorecombination has been studied at midinfrared laser fields [38], and the interplay between structural and dynamical interferences is found to modify the position of the minimum in the HH spectrum [39,40]. By measurements of HHG emission of CO_2, the underlying electronic dipole elements of the HHG signal and continuum electron dynamics are extracted [41], but the roles of multiple

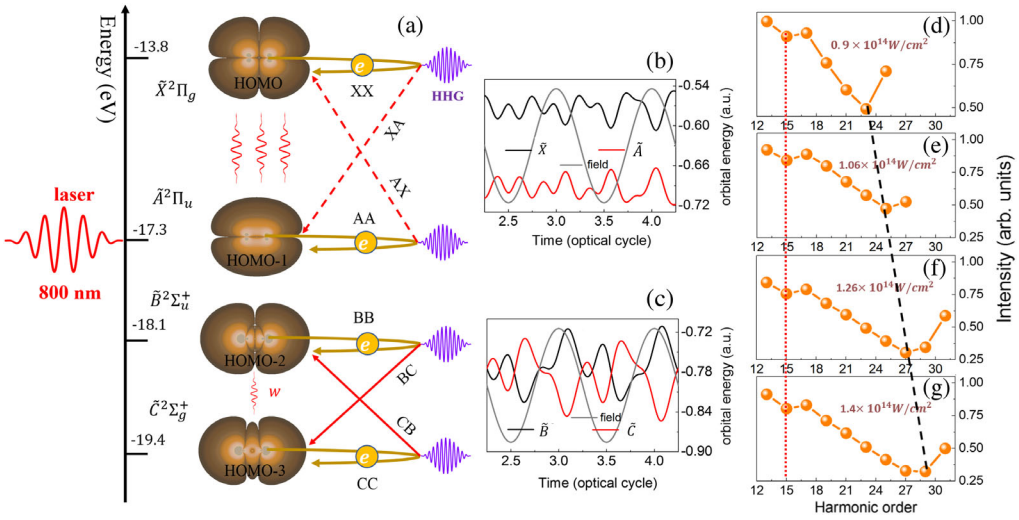

FIG. 1. (a) Orbital structures corresponding to different ionic states of CO_2 and the schematic layout for HHG involved multiple channels. Calculated time-dependent orbital energy of cationic states at $I = 1.26 \times 10^{14}$ W/cm^2, $\lambda = 800$ nm: (b) $\tilde{X}$ (black line) and $\tilde{A}$ (red line); (c) $\tilde{B}$ (black line) and $\tilde{C}$ (red line). The gray lines in (b) and (c) represent the laser field which has a trapezoidal envelope with a four-cycle flattop and one-cycle ramp for turn-on or turn-off. Measured harmonic spectra (integrated over each harmonic line) of CO_2 molecules aligned parallel to the polarization of the generating laser field for (d) $I = 0.9 \times 10^{14}$ W/cm^2, (e) $I = 1.06 \times 10^{14}$ W/cm^2, (f) $I = 1.26 \times 10^{14}$ W/cm^2, and (g) $I = 1.4 \times 10^{14}$ W/cm^2. The red dotted and black dashed lines indicate the positions of the minima of harmonic spectra [(d)–(g)].

orbitals are still unclear. Adopting two-color laser fields, the contribution of different orbitals can be resolved [42], and dynamical changes of the molecular orbital can be mapped onto the two-dimensional high-harmonic spectroscopy (HHS) of CO_2 [43]. Recently, the coupling between different channels left a mark in the two-dimensional HHS of CO_2, which can be used to reconstruct the relative phases and amplitudes for relevant ionization channels on a subcycle timescale [32].

In this Letter, we perform measurements of the HH spectra of aligned CO_2 molecules for different intensities. Two groups of spectral minimum structure are observed in CO_2, where one is independent of the laser intensity and another one shifts with intensity. *Ab initio* calculations of the HHG spectra of CO_2 by adopting time-dependent Hartree-Fock (TDHF) theory are in good agreement with the experimental results. Analysis shows that the cross-channel associated with two cationic states $\tilde{B}$ and $\tilde{C}$ (an electron is ionized from the HOMO-3) plays a vital role in shaping the molecular HHG spectrum, especially for the minimum structure in the lower-energy region. The laser-induced coupling between two cationic states $\tilde{B}$ and $\tilde{C}$ results in a situation where the relative phase between the channel involving cationic state $\tilde{X}$ and the coupling channel composed of two cationic states $\tilde{B}$ and $\tilde{C}$ is dependent on the momentum of the electron in the recombination process.

Figure 1(a) shows the Hartree-Fock orbitals corresponding to the ion CO_2^+ created in the ground state $\tilde{X}^2\Pi_g$ ($\tilde{X}$), first excited state $\tilde{A}^2\Pi_u$ ($\tilde{A}$), second excited state $\tilde{B}^2\Sigma_u^+$ ($\tilde{B}$), and third excited state $\tilde{C}^2\Sigma_g^+$ ($\tilde{C}$). If the state of the ion does not change between ionization and recombination, there are four channels: *XX*, *AA*, *BB*, and *CC*, where the first and second letters label the state of the ion after ionization and before recombination, respectively, as shown in Fig. 1(a). However, the laser field can couple the different ionic states between ionization and recombination and lead to additional cross-channels, which reflects the crucial impact of subcycle laser-induced dynamics and transitions on the harmonic radiation [31,32]. When the laser polarization is parallel to the molecular alignment, the cross-channels are simplified to *XA*, *AX*, *BC*, and *CB*. The laser frequency ($\omega = 1.55$ eV) used is close to the energy gap between the two ionic states $\tilde{B}$ and $\tilde{C}$ ($\omega_{\tilde{B}\tilde{C}} \approx 1.3$ eV). Thus, $\tilde{B}$ and $\tilde{C}$ are strongly coupled, and this coupling may leave fingerprints in the HHS. On the other hand, the energy gap between the two cationic states $\tilde{X}$ and $\tilde{A}$ ($w_{\tilde{A}\tilde{X}} \approx 3.5$ eV) is much larger than the laser frequency, and the ionization of HOMO-1 is suppressed along the molecular axis [36], so the contributions from channels *AA*, *XA*, and *AX* can be ignored when the molecule is aligned. Figure 1(b) shows the time-dependent orbital energies of cationic states $\tilde{X}$ (black line) and $\tilde{A}$ (red line) calculated by the TDHF equations [44] (see Supplemental Material for details [45]) at 800 nm and $I = 1.26 \times 10^{14}$ W/cm^2. The black and red curves in Fig. 1(c) represent the time-dependent orbital energies of the $\tilde{B}$ and $\tilde{C}$ cationic states, respectively, under the same laser parameters as Fig. 1(b). Comparing Fig. 1(b) with Fig. 1(c), we see that strong coupling exists between

the $\tilde{B}$ and $\tilde{C}$ states. Experimentally, the harmonic spectra in aligned CO_2 molecules at different laser intensities are shown in Figs. 1(d)–1(g). In our experiments, the output of a 35 fs, 800 nm laser facility is separated into two beams for nonadiabatic alignment of CO_2 molecules (the aligning laser) and generation of harmonics (the driving laser). The intensity of aligning laser is about 5×10^{13} W/cm^2. The two pulses are collinearly focused with an $f = 500$ mm spherical mirror into a supersonic gas jet of molecules. A home-built XUV flat-field grating spectrometer is used to measure the harmonic spectrum [57,58]. The harmonic spectrum of CO_2 is recorded at an aligned point (the delay time between two lasers of 21.1 ps). The degree of alignment $\langle \cos^2 \theta \rangle$ is estimated to be 0.55. The laser focus is placed before the gas jet in order to select the short trajectory harmonics [59,60]. Detailed information about the experimental setup can be found in Supplemental Material [45].

In Figs. 1(d)–1(g), two groups of minimum structure are presented. The minimum at the 15th order is independent of the laser intensities. Another group of minimum structure in the high-energy region shifts to higher orders with increasing intensity, which is attributed to dynamic interference between the diagonal channels XX and BB as proposed by Smirnova *et al.* [20], whereas the picture could be expected to be modified when the ionic states $\tilde{B}$ and $\tilde{C}$ are strongly coupled by the laser field.

To simulate the experiment, we coherently add the contributions from all channels involving cationic states $\tilde{X}$, $\tilde{A}$, $\tilde{B}$, and $\tilde{C}$, and the contributions of the long trajectories have been filtered out by applying a complex absorbing potential acting as a filter [29]. Figure 2(a) shows the harmonic spectra calculated for four valence orbitals in CO_2 exposed to a linear polarized laser field which has a trapezoidal envelope with a four-cycle flattop and one-cycle ramp for turn-on or turn-off. Here, our calculations qualitatively reproduce the two groups of spectral minimum observed experimentally in Figs. 1(d)–1(g). A minimum at H17 shows up for all laser intensities. In addition, dip structures appearing in higher-order regions are in good agreement with experimental observations. In Fig. 2(b), the calculated relative phase between the channels XX and $(B + C)$ are illustrated, where the channel $(B + C)$ that we call "coupling channel" includes both diagonal (BB and CC) and off-diagonal (BC and CB) channels. For each laser intensity, two interference minima approximately corresponding to a phase difference of π can be seen in the lower- and higher-order parts. The π radian minimum at lower energy [red arrow in Fig. 2(b)] is independent of the laser intensity, while the location of minimum at higher energy shifts to higher orders with increasing intensity. For comparison, we performed calculations with the time-dependent orbitals of three cationic states ($\tilde{X}$, $\tilde{A}$, and $\tilde{B}$), which is shown in Fig. 2(c). For all the laser conditions, the minimum in the lower-order region disappears.

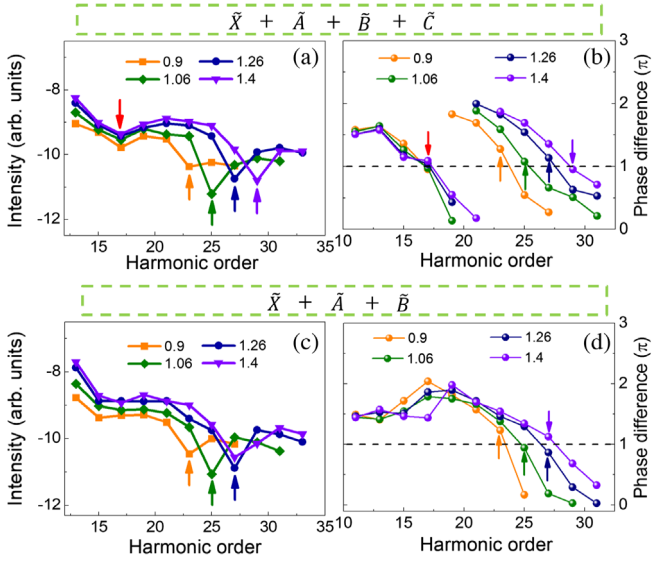

FIG. 2. Calculated harmonic spectra with the time-varying orbitals of cationic states for (a) four cationic states ($\tilde{X}$, $\tilde{A}$, $\tilde{B}$, and $\tilde{C}$) and (c) three cationic states ($\tilde{X}$, $\tilde{A}$, and $\tilde{B}$). Intensities are given in units of 10^{14} W/cm^2. (b) The phase difference between the channels XX and $(B + C)$ is calculated for four valence orbitals. (d) The phase difference between the channels XX and BB is calculated for three valence orbitals. The arrows mark the positions of the minima in HHG spectra.

The positions of interference minima located in the higher-order region are the same as the results in Fig. 2(a) in the laser intensity range from 0.9×10^{14} to 1.26×10^{14} W/cm^2, but the location for $I = 1.4 \times 10^{14}$ W/cm^2 is lower than the result from the coherent sum of four orbitals. The phase difference between the diagonal channels XX and BB is shown in Fig. 2(d). It can be seen that the phase difference is far from π in the lower-order part for all the laser intensities, consistent with the harmonic spectra in Fig. 2(c). The harmonic orders with relative phases of π [Fig. 2(d)] in the higher-order region correspond to the spectral minima in Fig. 2(c) for different laser intensities. The comparison between Figs. 2(a) and 2(b) and Figs. 2(c) and 2(d) clearly shows that the two groups of spectral minimum [Fig. 2(a)] result from the multichannel interference between XX and $(B + C)$ and emphasizes the importance of laser-driven coupling between the ionic states $\tilde{B}$ and $\tilde{C}$. In addition, for a laser field with a wavelength of 1500 nm, the minimum in the low-energy region disappears due to changed coupling between the ionic states $\tilde{B}$ and $\tilde{C}$ and relative contributions from different orbitals (see Supplemental Material [45] for details).

The purple and cyan lines in Fig. 3(a) represent the ionization and recombination times, respectively, of harmonic orders for a laser intensity of 1.26×10^{14} W/cm^2, which are calculated by the nonadiabatic classical-trajectory Monte Carlo (CTMC) model (see Supplemental Material [45] for details). The green and blue balls in

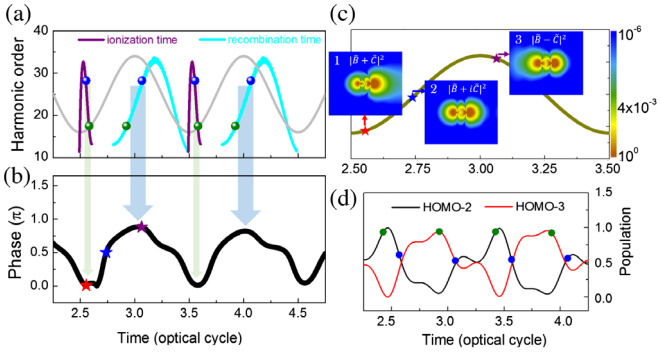

FIG. 3. (a) Ionization times (purple lines) and recombination times (cyan lines) calculated by the nonadiabatic CTMC model. (b) The time-dependent relative phase between the cationic states $\tilde{B}$ and $\tilde{C}$. See the text for the light green and blue arrows. (c) Visualization of the hole dynamics composed of a superposition of ionic states $\tilde{B}$ and $\tilde{C}$ with the relative phase $\varphi = 0$ (1), $\varphi = \pi/2$ (2), and $\varphi = \pi$ (3). (d) Populations of the time-dependent ionic state $\tilde{B}$ projecting on time-independent HOMO-2 (black line) and HOMO-3 (red line) of a CO_2 molecule. The gray and yellow lines in (a) and (c) represent the laser field with respect to time. The laser intensity is $I = 1.26 \times 10^{14}$ W/cm^2.

Fig. 3(a) label the ionization and recombination times of H17 and H27 from short trajectories, respectively. In the strongly coupled two-level system, two quasienergy states can be formed by the superposition of $\tilde{B}$ and $\tilde{C}$ ionic states. In Fig. 3(b), we show the relative phase between the cationic states $\tilde{B}$ and $\tilde{C}$ as a function of time for a laser intensity of 1.26×10^{14} W/cm^2. It is shown that the relative phase at the ionization times [the light green arrows in Fig. 3(b)] is approximately zero, while a phase difference of approximately π is observed at the recombination times [the light blue arrows in Fig. 3(b)]. This indicates that a quasienergy state $\psi_{\tilde{B}}(t) + \psi_{\tilde{C}}(t)$ is preferred in the ionization process in agreement with the result of Ref. [32], but the quasienergy state in the recombination process is $\psi_{\tilde{B}}(t) - \psi_{\tilde{C}}(t)$. Figure 3(c) shows the visualization of a superposition of the ionic states $\tilde{B}$ and $\tilde{C}$: $|\psi_{\tilde{B}}(t) + e^{i\varphi}\psi_{\tilde{C}}(t)|^2$, where φ represents the phase difference between $\tilde{B}$ and $\tilde{C}$. The snapshots show the hole density composed of two ionic states $\tilde{B}$ and $\tilde{C}$ at the times indicated by the stars corresponding to the phase differences $\varphi = 0$, $\pi/2$, and π.

Figure 3(d) shows the populations of time-varying ionic state $\tilde{B}$ projecting on the stationary states of HOMO-2 and HOMO-3 of a CO_2 molecule for a laser intensity of 1.26×10^{14} W/cm^2, where the green and blue dots indicate the recombination times of H17 and H27 obtained by nonadiabatic CTMC calculations, respectively. It can be seen that the composition of stationary state orbitals (HOMO-2 and HOMO-3) in the time-dependent cationic state $\tilde{B}$ accounts for about 50% at the recombination time of H27, while for H17 the time-varying ionic state $\tilde{B}$ is mainly composed by the stationary states HOMO-2 or HOMO-3 alternately at the recombination times (a similar result can be obtained for the ionic state $\tilde{C}$).

We recall that two main sources contribute to the phase difference between the channels: the evolution of the electronic states of the ion during the excursion time and the recombination phase [20]. For the coupling channel $(B + C)$ that is $\psi_{\tilde{B}}(t) - \psi_{\tilde{C}}(t)$ in the recombination process, the recombination matrix is $\mathbf{d}_{\mathrm{rec}}^{C} \propto i[\sin(\mathbf{P_2R}/2) + i\cos(\mathbf{P_3R}/2)]$ [45], where $\mathbf{R}$ is the internuclear vector and $\mathbf{P_2}$ and $\mathbf{P_3}$ are momentum vectors of recombination electrons captured by the ionic states $\tilde{B}$ and $\tilde{C}$, respectively. The recombination matrix of the channel XX is $\mathbf{d}_{\mathrm{rec}}^{XX} \propto i\sin(\mathbf{P_1R}/2)$ with the recombination momentum $\mathbf{P_1}$ of the electron. The phase difference between the diagonal channel XX and the coupling channel $(B + C)$ is dependent on the momenta of recombination electrons $\mathbf{P_1}$, $\mathbf{P_2}$, and $\mathbf{P_3}$. The momenta $\mathbf{P_2}$ and $\mathbf{P_3}$ are close to each other for the same harmonic order according to our calculation (see Supplemental Material [45]), so we can use the average value of $\mathbf{P_2R}/2$ and $\mathbf{P_3R}/2$ as the phase of the recombination matrix of the coupling channel. The relative phase between the two channels XX and $(B + C)$ can be approximated by

$$\triangle\varphi = I_p\tau - I_p^X\tau_X + \Phi, \tag{1}$$

where I_p is the average ionization energy $(I_p^B + I_p^C)/2$ with the ionization energies of molecular orbitals $(I_p^i, i = B, C)$; I_p^X is the ionization energy of HOMO; τ is the time interval between ionization and recombination for the coupling channel $(B + C)$, and τ_X is the excursion time of channel XX; and Φ is the recombination phase difference between XX and $(B + C)$ channels.

Figure 4(a) shows the excursion times of channels XX, BB, and CC calculated by the CTMC model. It is clearly

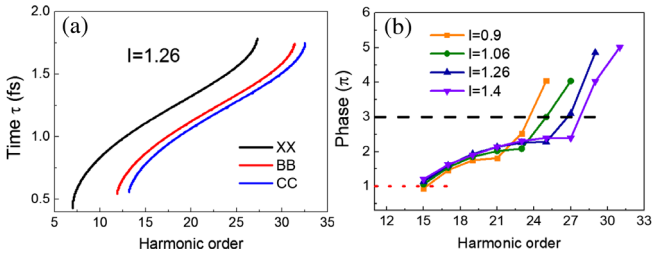

FIG. 4. Calculations of the nonadiabatic CTMC model. (a) The electron excursion times τ (short trajectories) associated with channels XX (black line), BB (red line), and CC (blue line), calculated for $I = 1.26 \times 10^{14}$ W/cm^2. (b) The relative phase according to Eq. (1) as a function of the harmonic order (short trajectories) for different laser intensities. Intensities are given in units of 10^{14} W/cm^2. The red dotted and black dashed lines indicate the phases of 1π and 3π, respectively.

seen that an approximate 240–330 as time lag between XX and BB (CC) exists for the same harmonic order. Thus, we apply different excursion times for different channels in Eq. (1). It is worthwhile mentioning that, in the higher-energy part beyond the cutoff of channel XX for each laser intensity, the excursion time of cutoff is used for τ_X of I_p^X. The locations of multichannel interference minima is predicted by the intersections of the black dashed line and solid lines in Fig. 4(b), which correspond to a phase difference of 3π shifts to higher order with intensity. In the lower-energy part, the intersections between the red dotted line and solid lines in Fig. 4(b) indicate an interference minimum located at about H15 which is independent of the laser intensity. These results are qualitatively consistent with the experimental observations and *ab initio* calculations.

In conclusion, measurements of harmonic spectra and TDHF simulation allow us to resolve multichannel coupling dynamics in molecular systems exposed to an intense laser field. In the case of CO_2, our theoretical and experimental results show that the observed two groups of minima result from the dynamical interference of the diagonal channel XX and the coupling channel ($B + C$). The interference minimum in the high-energy region of the spectrum shifts with intensity, and the interference minimum located in the lower-energy region is independent of the laser intensity. Our results reveal that these deeper-lying molecular orbitals can leave a clear fingerprint in the HHG spectra due to the coupling between channels. The sensitivity of HHG spectra to the deeper orbitals due to the laser-induced coupling of different ionic states provides the possibility of laser control of the inner-shell hole dynamics on the subcycle timescale.

This work was supported by the National Key program for S&T Research and Development (No. 2019YFA0307700), National Natural Science Foundation of China (Grants No. 91750104 and No. 11974137), the Key-Area Research and Development Program of Guangdong Province under Grant No. 2019B030330001, and the Science and Technology Program of Guangzhou (China) under Grant No. 201904020024.

*These authors contributed equally to this work.
†hushlin@mail.sysu.edu.cn
‡rma@jlu.edu.cn
§chen_jing@iapcm.ac.cn

[1] P. B. Corkum, Plasma Perspective on Strong Field Multiphoton Ionization, Phys. Rev. Lett. **71**, 1994 (1993).
[2] P. B. Corkum and F. Krausz, Attosecond science, Nat. Phys. **3**, 381 (2007).
[3] J. Itatani, J. Levesque, D. Zeidler, H. Niikura, H. Pépin, J. C. Kieffer, P. B. Corkum, and D. M. Villeneuve, Tomographic imaging of molecular orbitals, Nature (London) **432**, 867 (2004).
[4] S. Haessler, J. Caillat, W. Boutu, C. Giovanetti-Teixeira, T. Ruchon, T. Auguste, Z. Diveki, P. Breger, A. Maquet, B. Carré, R. Taïeb, and P. Salières, Attosecond imaging of molecular electronic wavepackets, Nat. Phys. **6**, 200 (2010).
[5] H. J. Wörner, J. B. Bertrand, D. V. Kartashov, P. B. Corkum, and D. M. Villeneuve, Following a chemical reaction using high-harmonic interferometry, Nature (London) **466**, 604 (2010).
[6] S. Ghimire, A. D. DiChiara, E. Sistrunk, P. Agostini, L. F. DiMauro, and D. A. Reis, Observation of high-order harmonic generation in a bulk crystal, Nat. Phys. **7**, 138 (2011).
[7] M. Hentschel, R. Kienberger, Ch. Spielmann, G. A. Reider, N. Milosevic, T. Brabec, P. Corkum, U. Heinzmann, M. Drescher, and F. Krausz, Attosecond metrology, Nature (London) **414**, 509 (2001).
[8] F. Krausz and M. Ivanov, Attosecond physics, Rev. Mod. Phys. **81**, 163 (2009).
[9] O. Smirnova, S. Patchkovskii, Y. Mairesse, N. Dudovich, and M. Yu. Ivanov, Strong-field control and spectroscopy of attosecond electron-hole dynamics in molecules, Proc. Natl. Acad. Sci. U.S.A. **106**, 16556 (2009).
[10] F. Calegari, D. Ayuso, A. Trabattoni, L. Belshaw, S. De Camillis, S. Anumula, F. Frassetto, L. Poletto, A. Palacios, P. Decleva, J. B. Greenwood, F. Martìn, and M. Nisoli, Ultrafast electron dynamics in phenylalanine initiated by attosecond pulses, Science **346**, 336 (2014).
[11] A. J. Uzan, H. Soifer, O. Pedatzur, A. Clergerie, S. Larroque, B. D. Bruner, B. Pons, M. Invanov, O. Smirnova, and N. Dudovich, Spatial molecular interferometry via multidimensional high-harmonic spectroscopy, Nat. Photonics **14**, 188 (2020).
[12] H. J. Wörner, H. Niikura, J. B. Bertrand, P. B. Corkum, and D. M. Villeneuve, Observation of Electronic Structure Minima in High-Harmonic Generation, Phys. Rev. Lett. **102**, 103901 (2009).
[13] A. D. Shiner, B. E. Schmidt, C. Trallero-Herrero, H. J. Wörner, S. Patchkovskii, P. B. Corkum, J-C. Kieffer, F. Légaré, and D. M. Villeneuve, Probing collective multielectron dynamics in xenon with high-harmonic spectroscopy, Nat. Phys. **7**, 464 (2011).
[14] M. Lein, N. Hay, R. Velotta, J. P. Marangos, and P. L. Knight, Role of the Intramolecular Phase in High-Harmonic Generation, Phys. Rev. Lett. **88**, 183903 (2002).
[15] S. Baker, J. S. Robinson, M. Lein, C. C. Chirilă, R. Torres, H. C. Bandulet, D. Comtois, J. C. Kieffer, D. M. Villeneuve, J. W. G. Tisch, and J. P. Marangos, Dynamic Two-Center Interference in High-Order Harmonic Generation from Molecules with Attosecond Nuclear Motion, Phys. Rev. Lett. **101**, 053901 (2008).
[16] T. Kanai, S. Minemoto, and H. Sakai, Quantum interference during high-order harmonic generation from aligned molecules, Nature (London) **435**, 470 (2005).
[17] C. Vozzi, F. Calegari, E. Benedetti, J.-P. Caumes, G. Sansone, S. Stagira, M. Nisoli, R. Torres, E. Heesel, N. Kajumba, J. P. Marangos, C. Altucci, and R. Velotta, Controlling Two-Center Interference in Molecular High Harmonic Generation, Phys. Rev. Lett. **95**, 153902 (2005).

[18] W. Boutu, S. Haessler, H. Merdji, P. Breger, G. Waters, M. Stankiewicz, L. J. Frasinski, R. Taieb, J. Caillat, A. Maquet, P. Monchicourt, B. Carre, and P. Salieres, Coherent control of attosecond emission from aligned molecules, Nat. Phys. **4**, 545 (2008).

[19] X. Zhou, R. Lock, W. Li, N. Wagner, M. M. Murnane, and H. C. Kapteyn, Molecular Recollision Interferometry in High Harmonic Generation, Phys. Rev. Lett. **100**, 073902 (2008).

[20] O. Smirnova, Y. Mairesse, S. Patchkovskii, N. Dudovich, D. Villeneuve, P. Corkum, and M. Yu. Ivanov, High harmonic interferometry of multi-electron dynamics in molecules, Nature (London) **460**, 972 (2009).

[21] M. R. Miller, A. Jaroń-Becker, and A. Becker, High-harmonic spectroscopy of laser-driven nonadiabatic electron dynamics in the hydrogen molecular ion, Phys. Rev. A **93**, 013406 (2016).

[22] M. R. Miller, Y. Xia, A. Becker, and A. Jaroń-Becker, Laser-driven nonadiabatic electron dynamics in molecules, Optica **3**, 259 (2016).

[23] B. K. McFarland, J. P. Farrell, P. H. Bucksbaum, and M. Gühr, High harmonic generation from multiple orbitals in N_2, Science **322**, 1232 (2008).

[24] D. Shafir, H. Soifer, B. D. Bruner, M. Dagan, Y. Mairesse, S. Patchkovskii, M. Yu. Ivanov, O. Smirnova, and N. Dudovich, Resolving the time when an electron exits a tunnelling barrier, Nature (London) **485**, 343 (2012).

[25] J. B. Bertrand, H. J. Wörner, P. Salières, D. M. Villeneuve, and P. B. Corkum, Linked attosecond phase interferometry for molecular frame measurements, Nat. Phys. **9**, 174 (2013).

[26] Y. Huang, J. Zhao, Z. Shu, Y. Zhu, J. Liu, W. Dong, X. Wang, Z. Lü, D. Zhang, J. Yuan, J. Chen, and Z. Zhao, Ultrafast hole deformation revealed by molecular attosecond interferometry, Ultrafast Sci. **2021**, 9837107 (2021).

[27] R. Santra and A. Gordon, Three-Step Model for High-Harmonic Generation in Many-Electron Systems, Phys. Rev. Lett. **96**, 073906 (2006).

[28] S. Patchkovskii, Z. Zhao, T. Brabec, and D. M. Villeneuve, High Harmonic Generation and Molecular Orbital Tomography in Multielectron Systems: Beyond the Single Active Electron Approximation, Phys. Rev. Lett. **97**, 123003 (2006).

[29] S. Sukiasyan, C. McDonald, C. Destefani, M. Yu. Ivanov, and T. Brabec, Multielectron Correlation in High-Harmonic Generation: A 2D Model Analysis, Phys. Rev. Lett. **102**, 223002 (2009).

[30] A. Ferré *et al.*, Multi-channel electronic and vibrational dynamics in polyatomic resonant high-order harmonic generation, Nat. Commun. **6**, 5952 (2015).

[31] Y. Mairesse, J. Higuet, N. Dudovich, D. Shafir, B. Fabre, E. Mével, E. Constant, S. Patchkovskii, Z. Walters, M. Yu.Ivanov, and O. Smirnova, High Harmonic Spectroscopy of Multichannel Dynamics in Strong-Field Ionization, Phys. Rev. Lett. **104**, 213601 (2010).

[32] B. D. Bruner, Z. Mašín, M. Negro, F. Morales, D. Brambila, M. Devetta, D. Faccialà, A. G. Harvey, M. Ivanov, Y. Mairesse, S. Patchkovskii, V. Serbinenko, H. Soifer, S. Stagira, C. Vozzi, N. Dudovich, and O. Smirnova, Multidimensional high harmonic spectroscopy of polyatomic molecules: Detecting sub-cycle laser-driven hole dynamics upon ionization in strong mid-IR laser fields, Faraday Discuss. **194**, 369 (2016).

[33] Z. Diveki, R. Guichard, J. Caillat, A. Camper, S. Haessler, T. Auguste, T. Ruchon, B. Carré, A. Maquet, R. Taïeb, and P. Salières, Molecular orbital tomography from multichannel harmonic emission in N_2, Chem. Phys. **414**, 121 (2013).

[34] D. Pavičić, K. F. Lee, D. M. Rayner, P. B. Corkum, and D. M. Villeneuve, Direct Measurement of the Angular Dependence of Ionization for N_2, O_2, and CO_2 in Intense Laser Fields, Phys. Rev. Lett. **98**, 243001 (2007).

[35] M. Spanner and S. Patchkovskii, One-electron ionization of multielectron systems in strong nonresonant laser fields, Phys. Rev. A **80**, 063411 (2009).

[36] S. Petretti, Y. V. Vanne, A. Saenz, A. Castro, and P. Decleva, Alignment-Dependent Ionization of N_2, O_2, and CO_2 in Intense Laser Fields, Phys. Rev. Lett. **104**, 223001 (2010).

[37] V. P. Majety and A. Scrinzi, Dynamic Exchange in the Strong Field Ionization of Molecules, Phys. Rev. Lett. **115**, 103002 (2015).

[38] C. Vozzi, M. Negro, F. Calegari, G. Sansone, M. Nisoli, S. De Silvestri, and S. Stagira, Generalized molecular orbital tomography, Nat. Phys. **7**, 822 (2011).

[39] H. J. Wörner, J. B. Bertrand, P. Hockett, P. B. Corkum, and D. M. Villeneuve, Controlling the Interference of Multiple Molecular Orbitals in High-Harmonic Generation, Phys. Rev. Lett. **104**, 233904 (2010).

[40] R. Torres, T. Siegel, L. Brugnera, I. Procino, J. G. Underwood, C. Altucci, R. Velotta, E. Springate, C. Froud, I. C. E. Turcu, S. Patchkovskii, M. Yu. Ivanov, O. Smirnova, and J. P. Marangos, Revealing molecular structure and dynamics through high-order harmonic generation driven by mid-IR fields, Phys. Rev. A **81**, 051802(R) (2010).

[41] R. M. Lock, S. Ramakrishna, X. Zhou, H. C. Kapteyn, M. M. Murnane, and T. Seideman, Extracting Continuum Electron Dynamics from High Harmonic Emission from Molecules, Phys. Rev. Lett. **108**, 133901 (2012).

[42] H. Yun, K.-M. Lee, J. H. Sung, K. T. Kim, H. T. Kim, and C. H. Nam, Resolving Multiple Molecular Orbitals Using Two-Dimensional High-Harmonic Spectroscopy, Phys. Rev. Lett. **114**, 153901 (2015).

[43] H. Niikura, N. Dudovich, D. M. Villeneuve, and P. B. Corkum, Mapping Molecular Orbital Symmetry on High-Order Harmonic Generation Spectrum Using Two-Color Laser Fields, Phys. Rev. Lett. **105**, 053003 (2010).

[44] S.-L. Hu, Z.-X. Zhao, J. Chen, and T.-Y. Shi, Ionization dynamics of C_2H_2 in intense laser fields: Time-dependent Hartree-Fock approach, Phys. Rev. A **92**, 053409 (2015).

[45] See Supplemental Material at http://link.aps.org/supplemental/10.1103/PhysRevLett.128.183202 for the details of the TDHF method, nonadiabatic CTMC model, and the experimental setup, which includes Refs. [46–56].

[46] E. Löstedt, T. Kato, and K. Yamanouchi, Intramolecular electron dynamics in the ionization of acetylene by an intense laser pulse, J. Chem. Phys. **138**, 104304 (2013).

[47] S.-L. Hu, Z.-X. Zhao, and T.-Y. Shi, B-spline one-center method for molecular Hartree-Fock calculations, Int. J. Quantum Chem. **114**, 441 (2014).

[48] U. De Giovannini, A. H. Larsen, and A. Rubio, Modeling electron dynamics coupled to continuum states in finite volumes with absorbing boundaries, Eur. Phys. J. B **88**, 56 (2015).

[49] G. L. Kamta and A. D. Bandrauk, Three-dimensional time-profile analysis of high-order harmonic generation in molecules: Nuclear interferences in H_2^+, Phys. Rev. A **71**, 053407 (2005).

[50] J. J. Carrera, X. M. Tong, and Shih-I Chu, Creation and control of a single coherent attosecond XUV pulse by few-cycle intense laser pulses, Phys. Rev. A **74**, 023404 (2006).

[51] M. Li, J.-W. Geng, M. Han, M.-M. Liu, L.-Y. Peng, Q. Gong, and Y. Liu, Subcycle nonadiabatic strong-field tunneling ionization, Phys. Rev. A **93**, 013402 (2016).

[52] Q. Gao, S. Chen, H. Liang, Y. Wang, C. Bi, S. Ben, Ri Ma, D. Ding, and J. Chen, Comparison study on atomic and molecular ellipticity dependence of high-order harmonic generation, Phys. Rev. A **103**, 043115 (2021).

[53] W. Chu, M. Wu, B. Zeng, J. Yao, J. Ni, H. Xiong, H. Xu, Z. Lin, H. Kang, W. Quan, J. Chen, X. Liu, Y. Cheng, and Z. Xu, Unexpected breakdown of the simple man's model for strong-field photoionization in the high-energy recollision region, Phys. Rev. A **85**, 021403(R) (2012).

[54] C. C. Chirilă and M. Lein, Assessing different forms of the strong-field approximation for harmonic generation in molecules, J. Mod. Opt. **54**, 1039 (2007).

[55] J. C. Baggesen and L. B. Madsen, On the dipole, velocity and acceleration forms in high-order harmonic generation from a single atom or molecule, J. Phys. B **44**, 115601 (2011).

[56] A. Rupenyan, P. M. Kraus, J. Schneider, and H. J. Wörner, High-harmonic spectroscopy of isoelectronic molecules: Wavelength scaling of electronic-structure and multielectron effects, Phys. Rev. A **87**, 033409 (2013).

[57] Y. Niu, H.-J. Liang, Y. Liu, F.-Y. Liu, R. Ma, and D.-J. Ding, A tunable XUV monochromatic light source based on the time preserving grating selection of high-order harmonic generation, Chin. Phys. B **26**, 074222 (2017).

[58] H.-J. Liang, X. Fan, S. Feng, L.-Y. Shan, Q.-H. Gao, B. Yan, R. Ma, and H.-F. Xu, Quantum interference of multi-orbital effects in high-harmonic spectra from aligned carbon dioxide and nitrous oxide, Chin. Phys. B **28**, 094207 (2019).

[59] P. Salières, A. L'Huillier, and M. Lewenstein, Coherence Control of High-Order Harmonics, Phys. Rev. Lett. **74**, 3776 (1995).

[60] P. Antoine, A. L'Huillier, and M. Lewenstein, Attosecond Pulse Trains Using High–Order Harmonics, Phys. Rev. Lett. **77**, 1234 (1996).